applied sciences

MDPI

Article

Study on Preparation and Rheological Properties of 3D Printed Pre-Foaming Concrete

Yanan Gao, Sudong Hua * and Hongfei Yue

College of Material Science & Engineering, Nanjing Tech University, Nanjing 211816, China
* Correspondence: huasudong@126.com

Abstract: The high fluidity and low yield stress of fresh foam concrete affect the shape stability and buildability of foam concrete in the printing process, which is quite a challenge to its application in digital construction. Therefore, this article proposes the preparation and characteristics of 3D printed pre-foaming concrete (3DFC). The rheological properties proved that the addition of 0.1 wt.% Hydroxypropyl methyl cellulose (HPMC) to 3DFCs weakens the fluidity but increases the static yield stress and apparent viscosity, thus enhancing the buildability. More importantly, the influences of surfactant on the rheological property, compressive strength, pore structure and thermal conductivity of 3DFCs were evaluated. Analysis results show that the static yield stress of 3DFCs decreases from 1735 to 687 Pa with surfactant dosage from 0 to 2 wt.%. Moreover, the addition of surfactant significantly reduced the apparent viscosity of 3DFCs (especially at low shear rates), but its viscosity recovery rate was basically unchanged, which is good for buildability. Thanks to the increase of porosity, the volume density of 3DFCs decreased from 2211 to 1159 kg/m^3, but the compressive strength of 3DFCs also decreased slightly. The thermal conductivity of 3DFCs shows good thermal insulation performance in the range of 0.2254–0.2879 W/m·K, which is also due to the increase in porosity of 3DFCs. Finally, in order to verify the practical application value of 3DFCs, an industrial printing product with more than 30 layers during the field application is displayed.

Keywords: surfactant; 3D printed pre-foaming concrete; rheology; porosity; thermal conductivity

Citation: Gao, Y.; Hua, S.; Yue, H. Study on Preparation and Rheological Properties of 3D Printed Pre-Foaming Concrete. *Appl. Sci.* **2023**, *13*, 5303. https://doi.org/10.3390/app13095303

Academic Editor: Laurent Daudeville

Received: 16 March 2023
Revised: 9 April 2023
Accepted: 14 April 2023
Published: 24 April 2023

1. Introduction

Additive manufacturing in construction is one of the latest development trends in the concrete prefabrication industry [1,2]. This technology does not require formwork construction, greatly reduces labor costs, shortens construction time and brings extensive benefits to the construction industry [3,4]. At the same time, 3D-printed concrete based on extrusion molding is developing rapidly. Academic researchers and industry practitioners have developed printing concrete with good thixotropy; that is, materials maintain high yield stress in a static state and low viscosity after shear [5,6]. However, due to the high self weight of traditional 3D printing materials, there are huge costs in raw materials, transportation and labor. In addition, the dense wall with high thermal conductivity accelerates the indoor and outdoor heat loss, which is not conducive to the sustainable development of the environment. Therefore, it is urgent to develop an environment-friendly 3D printing material with light weight, porous and excellent thermal insulation effects [7].

One of the most significant sources of greenhouse gas emissions of carbon dioxide is the construction industry, which emits more than 40% of global emissions over its entire life cycle. With the development of the global concept of "carbon neutral", many scholars began to devote themselves to the development of low-density and energy-saving building materials [8]. Based on a surfactant and prefabricated foaming method, pre-foaming concrete has been recognized by practitioners in the industry [9,10]. Foamed concrete is a kind of lightweight porous material, which is formed by mixing a foaming agent with high-speed mechanical mixing and then pouring and curing foam into the mixed

mortar [11,12]. Due to the honeycomb porous structure, foam concrete has low-density, high fluidity, self-compacting and perfect thermal performance. Among them, the density can range from 300 to 1800 kg/m^3, and the thermal conductivity can range from 0.131 to 0.52 W/(m·K) which is only 10–50% of that of ordinary dense concrete [13–15]. It can be easily pumped to the construction position, which brings significant convenience to the construction industry. At present, the digital construction wall adopts the method of multi-layer printing and superposition to strengthen the bearing and improve the effect of thermal insulation and sound insulation. This means that the strength requirements for inner materials are not so high, which provides the possibility for the development and application of lightweight foams. If energy-saving materials with low thermal conductivity are used in inner thermal insulation walls, the thermal insulation capacity of the building can be greatly improved [16].

Extrusion-based 3D printing molding technology consists of four main stages, i.e., mixing, pumping, extrusion and construction [17]. Due to this special processing, the rheological properties of the printing ink are required differently in different stages. Low yield stress and apparent viscosity are required in the pumping and extrusion stages [18,19]. However, when the paste is extruded, high yield strength is required to resist the load from the subsequent build-up layer. In order to meet this challenge, many researchers have made a series of studies. Hussam Alghamdi et al. prepared 3D printable foam fly ash-based geopolymer matrices with surfactant [20]. The porosity of extruded geopolymeric foams was in the range of 55 to 75% for densities from 0.6 to 1.0 kg/m^3. Compared with the cast concrete in the same density range, these properties are very similar. However, the thermal conductivity of the foaming matrix is still very high, ranging from 0.15 W/(m·K) to 0.25 W/(m·K), which is due to the small pore in the foam and the large spacing between the printing paths. Devid Falliano et al. also prepared cement-based three-dimensional printable lightweight foam concrete using protein surfactants, and the resulting 3DP-LWFC had higher compressive strength than C-LWFC [21]. The mechanical strength of 3DP-LWFC increased with increasing dry density, which is similar to the C-LWFC. However, traditional foam concrete is difficult to use to meet the printing requirements, which are mainly manifested as higher fluidity and lower yield stress. Previous studies have shown that the rheological properties (yield stress and apparent viscosity) of foamed concrete are closely related to water incorporation [22]. In this experiment, the yield stress of the material is effectively increased by reducing the water–cement ratio. Additionally, Feneuil et al. provide clear insight into the effects of surfactant on the yield stress of OPC pastes [23]. They showed that the anionic surfactant that becomes adsorbed to the cement grain surface, depending on the concentration, can either increase or reduce the paste's yield stress; i.e., a lower concentration increases the yield stress whereas a higher concentration decreases the yield stress. Therefore, it is bold to guess that different foam content is also the main factor affecting the rheological properties of the "printing ink", thereby affecting the printing performance of the material.

The development of 3D printed pre-foaming concrete for construction is still at a relatively early stage. Not enough has been reported about the relationship between the composition, structure and properties of this lightweight printed mortar. The purpose of this paper is to investigate the essential properties of 3DFCs, including rheology, buildability, mechanical strength and thermal conductivity. An in-depth understanding of these problems is conducive to the practical application of lightweight thermal insulation mortar in digital construction.

2. Materials and Methods

2.1. Materials

The 42.5 ordinary Portland cement used in this experiment was provided by Anhui Conch Cement Ltd. (Anhui, China) The specific surface area is 325 m^2/kg, and the main chemical composition determined by X-ray fluorescence (XRF) is shown in Table 1. To improve the buildability and mechanical properties of the slurry, hydroxypropyl methyl

cellulose (HPMC) and polypropylene fiber (PP) are added to the paste, which were provided by Jiangsu Zhaojia Building Materials Technology Ltd. (Suzhou, China) and Guangzhou Schneider building materials Ltd. (Guangzhou, China) Natural river sand with a maximum particle size of 0.6 mm was provided by Jiangsu Yanghe Xincheng New Material Ltd. (Suqian, China) Foaming agent is a plant protein surfactant sold by Weihai Zhongsheng New Building Materials Co., Ltd. (Weihai, China), which is a yellowish liquid and diluted with water at 1:60.

Table 1. The main chemical compositions of cement. Lol is loss on ignition at 1000 °C (wt.%).

SiO_2	Al_2O_3	Fe_2O_3	TiO_2	CaO	MgO	SO_3	K_2O	Na_2O	MnO	P_2O_5	LOI
22.84	7.14	3.76	0.38	56.24	2.07	2.03	0.74	0.13	0.17	0.099	4.14

2.2. Mix Design and Preparation of Pastes

Table 2 shows the different mix proportions used in this study. Six mixes of 3D printed concrete were designed and manufactured to examine the effects of surfactant addition on the rheological and mechanical properties. First of all, the prepared powder was mixed for 5 min and then mixed with water to form a uniform slurry. The surfactant is diluted by water to a ratio of 1:60, and foams are produced by a pneumatic foam generator. Then, the foam is weighed and immediately transferred to the slurry to continue stirring for 1–2 min until the white foam disappears [24]. Low-speed mixing is used in the stirring process to avoid foam bursting during high-speed mixing. The prepared paste is used for follow-up experiments. Since the slurry does not have the basic printing performance, when the surfactant content exceeds 2%, the amount of surfactant in the range (0–2%) was experimented with.

Table 2. The mixture proportions of Blank and 3DFCs.

Mix	Cement	Admixture		Surfactant (%)	Water-Binder Ratio	SAND-Binder Ratio
		HPMC(%)	PP(%)			
Blank	100	0	0.2	0.5	0.4	1.1
3DFC0	100	0.1	0.2	0	0.4	1.1
3DFC0.5	100	0.1	0.2	0.5	0.4	1.1
3DFC1.0	100	0.1	0.2	1.0	0.4	1.1
3DFC1.5	100	0.1	0.2	1.5	0.4	1.1
3DFC2.0	100	0.1	0.2	2.0	0.4	1.1

2.3. 3D Printing Concrete

A HC-30PRT Concrete (Mortar) 3D Printing System is used to print the foam specimens. The initial printing parameters used in this study are presented as follows: layer height of 10mm, nozzle diameter of 20 mm, extrusion width of 9 mm, horizontal movement speed of 35 mm/s, vertical lifting rate of 5 mm/s and extrusion speed of 1.0 rad/s. In the 3D printing experiment of concrete, the buildability of printing mortar is evaluated by the number of printing layers. The stirred mortar is injected into the storage cylinder, and the mortar is extruded continuously and uniformly through the nozzle under the action of external force. The maximum number of printing layers before the collapse of the printed specimen was recorded, and the average value was taken from the three tests.

2.4. Experimental Methods of Fresh Foam Mortar

2.4.1. Mini-Slump and Fluidity

Fluidity is one of the important parameters to evaluate the pumpability and extrudability of 3D printed pre-foaming concrete, which is measured by cement mortar fluidity tester [25]. According to the standard ASTM C1437-15 [26], the fresh foam mortar is loaded into the truncated cone die, and then the truncated cone die is gently lifted. Then, the

jumping table is immediately activated and jumps 25 times. The expansion diameter (as shown in Figure 1a) of fresh foam mortar in two directions perpendicular to each other is recorded, and the average value is recorded as the fluidity of the 3DFCs. In order to directly reflect the buildability of 3DFCs, a mini-slump experiment was developed. The truncated cone die in fluidity experiment is used as an important tool for the mini-slump experiment [27]. After the fresh foam mortar is loaded into the truncated cone die, the truncated cone die is lifted slowly along the vertical direction. Then, the vertical distance (as shown in Figure 1b) from the highest point to the lowest point of fresh foam mortar is recorded from three angles, and the average value is recorded as the mini-slump of 3DFCs.

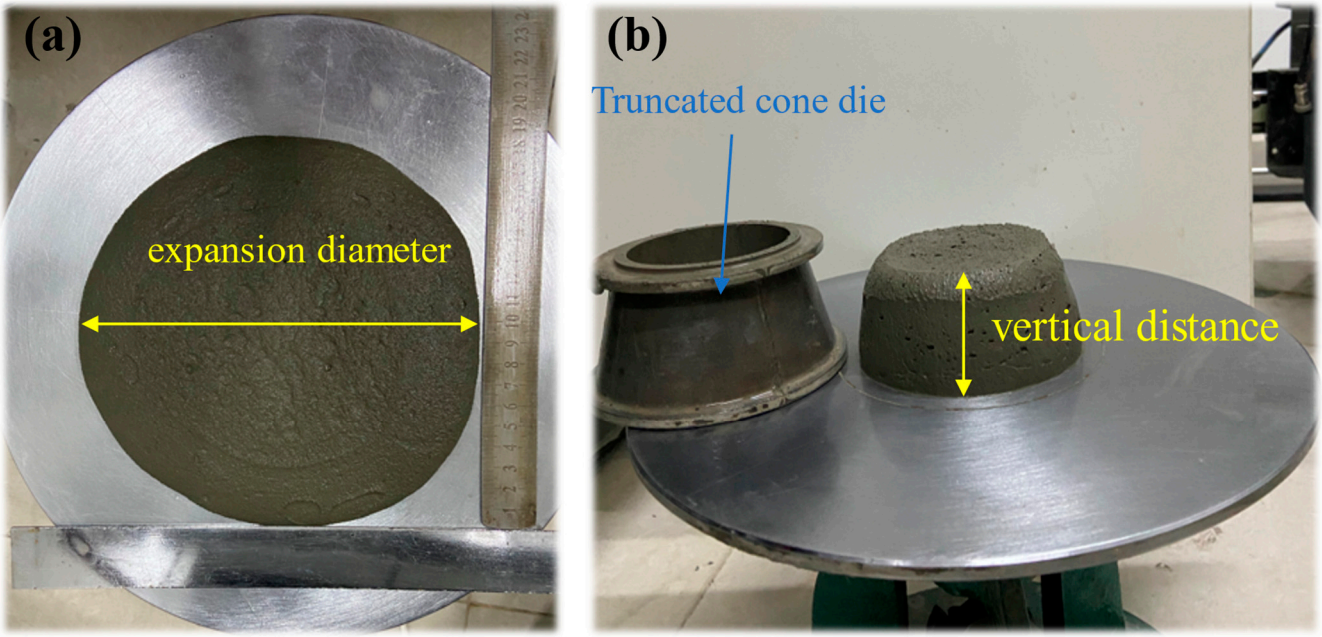

Figure 1. Photos showing the (**a**) mini-slump and (**b**) fluidity test.

2.4.2. Rheology

The characterization of the rheological of the fresh foam mortar was measured by a Brookfield rheometer (R/SP-SST), see Figure 2, which works by changing the shear rate (or rotational speed) [28]. After the fresh foam mortar is evenly stirred, it is transferred to the rheometer cup. The upper interface of the fresh foam mortar is flush with the scale line in the rheometer cup. The rheometer cup is placed in a rotary rheometer, and then the 4-blade vane probe is lowered slowly until it is completely passed by the fresh foam mortar. The rheological test was carried out with circulating water device at 20 °C.

The rheological testing mechanism mainly includes the following three steps: (I) Static yield stress test: Constant shear rate of 0.2 s^{-1} is applied to the foam sample for 120 s [29,30]. The low shear rate is for minimizing the effect of viscosity on the measured stress, which is almost negligible. (II) Viscosity recovery test (build-ability), as shown in Figure 3: First, the static viscosity of foam mortar is measured at the low shear rate of 0.01 s^{-1} for 50 s (stage (i)), and then the shear rate is rapidly increased and maintains a constant shear rate of 50 s^{-1} for 50 s (stage (ii)), and finally the shear rate is decreased rapidly and continues for 50 s at a low shear rate of 0.01 s^{-1} (stage (iii)). (III) Apparent viscosity test: The shear rate of rotary rheometer increased from 0 s^{-1} to 60 s^{-1} in 112 s, and the apparent viscosity of fresh foam mortar was measured with shear rate. The shear rate and corresponding time used in the above three processes are designed to simulate the 3D printing process, as described in Ref. [31].

Figure 2. Rheometer used in this study.

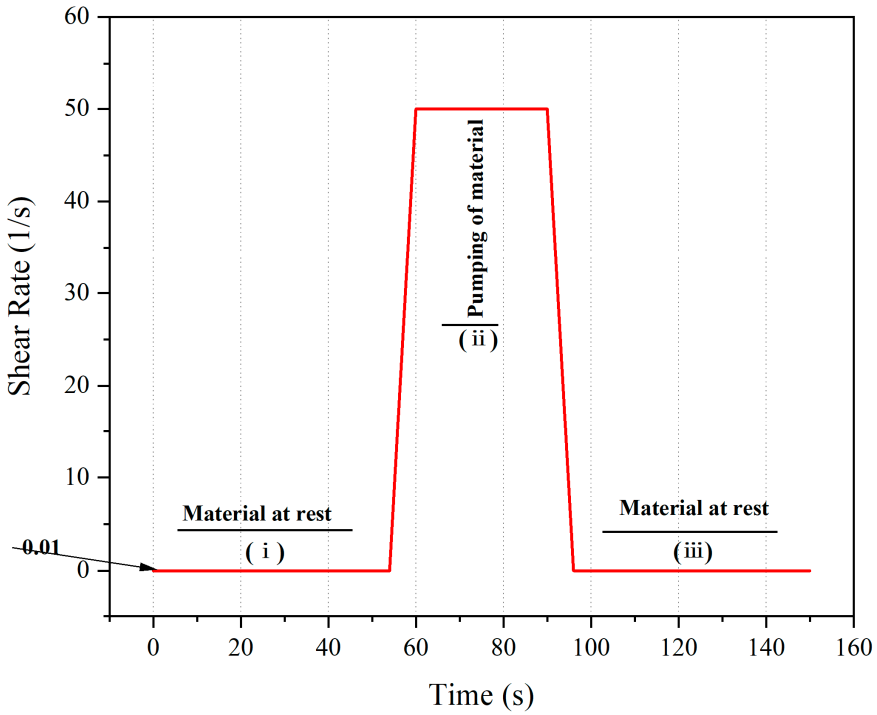

Figure 3. Viscosity recovery test.

2.5. Experimental Methods of Hardened Foam Mortar

2.5.1. Compressive Strength and Volume Density

According to the standard ASTM C349-18 [32], the WHY-200 Auto Test Compression Machine with a loading rate of 1 mm/min is used to test the compressive strength of 3DFCs. The extrusion speed of the printer is adjusted to 1.3 rad/s, and the compressive strength is tested by printing a rectangular test block of 40 × 40 × 160 mm. The volume densities of the printing suspensions with different contents of surfactant are measured by a WLD-1203MD Electronic Density Measuring Instrument. All the samples are cured at

room temperature (20 + 2 °C) for 28 days. Three repeated samples in each group are used to test.

2.5.2. Mercury Intrusion Porosimetry

The pore structures of the 28-day cured samples were characterized by a GT-60 Mercury Intrusion Porosimetry (MIP) (Quantachrome Instruments, Boynton, FL, USA). For the MIP experiment, the hardened foamed pastes were crushed into small granular samples with a size of about 2–3 mm and then stored in absolute alcohol for at least 24 h to stop the hydration reaction. All samples need to be dried in a 40 °C vacuum oven for 12 h before testing.

2.5.3. Scanning Electron Microscopy

In the hydration reaction terminated by anhydrous ethanol, the foam mortar was dried in a vacuum oven at 40 °C for 12 h. The dried sample is cut into square slices with a side length of about 5 mm. The pore structure of foam mortar was observed by a JSM- 6510 (Tokyo, Japan) scanning electron microscope. Before the test, the sample is sprayed with a thin layer of conductive gold.

2.5.4. Thermal Conductivity

The thermal conductivity of 3DP-LWFC at room temperature was measured by Lambda's HFM436 Thermal conductivity Meter. The specimens for testing thermal conductivity were prepared with a 150 × 150 × 20 mm resin mold and cured at room temperature for 28 days. In order to ensure good contact between the equipment and the sample surface, all samples were polished flat and parallel and cleaned with compressed air. So as to avoid the effect of sample humidity on thermal conductivity, the sample was dried in a vacuum drying box at 60 °C for 4 h before testing. The average value with standard deviation error of 3DFCs was acquired by testing three replicated samples.

3. Results and Discussion

3.1. Mini-Slump and Fluidity

The printability of 3D printed pre-foaming concretes (3DFCs) is decreased with the ability to be smoothly transported in the pipeline and extruded from the nozzle and maintain its shape stability. Workability (including fluidity and mini-slump) is one of the important properties to evaluate the printability of 3DFCs. Figure 4 shows the results of mini-slump and fluidity of a blank sample and 3DFCs. It can be observed that the initial fluidity of the blank sample is 196 mm, but its mini-slump is only 28 mm. Under these conditions, the mortar can be transported smoothly through the pipeline to the nozzle, but the shape stability cannot be maintained after extrusion. By adding 0.1% HPMC, the fluidity of sample 3DFC0.5 decreased to 140 mm, but its mini-slump increased to 56 mm. At this time, the sample 3DFC0.5 has good extrudability and buildability. When the surfactant increases from 0 to 2%, the initial fluidity of 3DFCs increases from 128 mm to 145 mm, and the mini-slump decreases from 57 mm to 53 mm. Past fluidity tests show that the fluidity range of ordinary mortar meeting the requirements of 3D printing is 175–205 mm. Combined with Figure 4, it can be seen that the fluidity of the sample 3DFC0 without surfactant obviously does not meet the printability for 3D printing. However, for 3DFCs mixed with surfactants, even a lower initial fluidity can still meet the printing requirements and maintain good buildability of 3D printing. This may be related to the loose and porous internal structure, which contributes to the smooth transportation of 3DFCs when additional pressure is required.

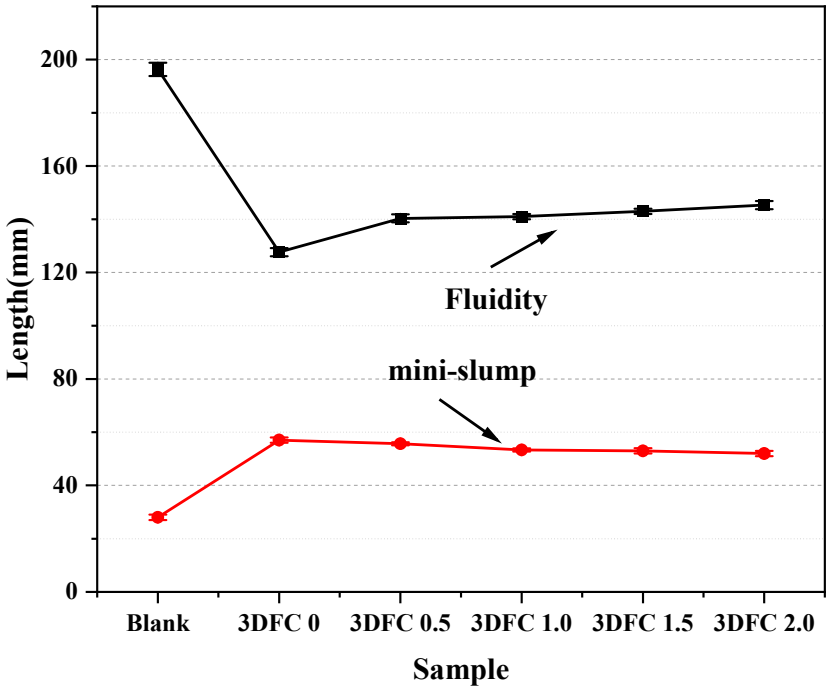

Figure 4. Fluidity and Mini-slump of Blank and 3DFCs.

Figure 5 shows the fluidity loss and mini-slump gain of 3DFCs over time. As shown in Figure 5, compared to the blank, the addition of 0.1 wt.% HPMC in 3DFCs can significantly decrease the fluidity loss within 2 h. Accordingly, the mini-slump gain also decreases over time, which is still good for buildability. Based on this, the fluidity loss and mini-slump gain caused by the change of surfactant content are small. This shows that the 3DFCs mixed with surfactant have good slump retention performance. For long-term site construction, it is undoubtedly beneficial to pump and print.

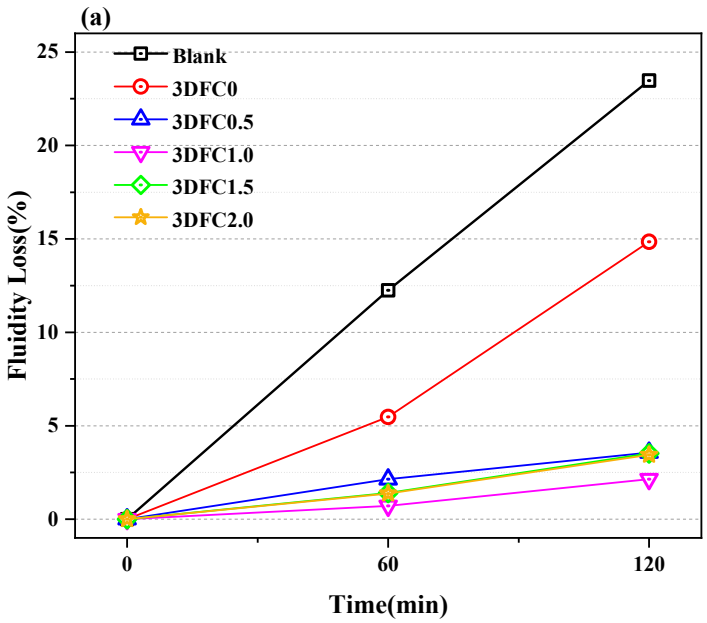

Figure 5. *Cont.*

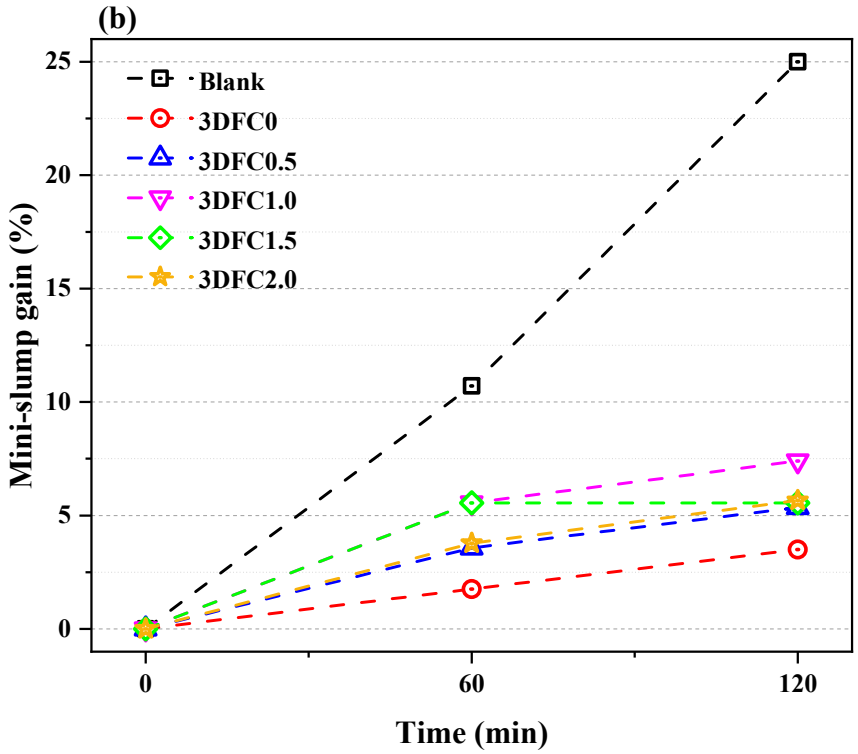

Figure 5. The (**a**) fluidity loss and (**b**) Mini-slump gain of blank and 3DFCs over time.

3.2. Static Yield Stress

Three-dimensional printing is a layer-by-layer superposition process. Each layer needs to have sufficient yield stress to resist the upper pressure without deformation. At a constant shear rate, the yield stress of the mixtures varies with time as shown in Figure 6. It can be seen from Figure 6 that the static yield stress of the blank is 183.543 Pa. However, under the same surfactant content, the static yield stress of 3DFC0.5 mixed with HPMC increases to 1189.998 Pa, which is about six times that of the blank. The addition of HPMC can effectively improve the static yield stress of foamed mortar. The sample 3DFC0 without surfactant shows the highest static yield stress of 1735.109 Pa, which is much higher than that of the sample with surfactant. When the content of surfactant is from 0.5% to 2.0%, the static yield stress decreases from 1189 to 687 Pa. Some studies have interpreted this change as the result of the competition between the skeleton yield stress of 3DFCs and bubble surface tension. To better evaluate this phenomenon, a plastic capillary number was introduced to quantify the balance between capillary forces and fluid stresses Equation (1) [33]:

$$\mathrm{Ca}_{\tau} = \frac{\tau}{2\mathrm{T}/\mathrm{R}} \quad (1)$$

where τ is the paste's yield stress that tends to deform the bubbles ; T is the capillary stress that tends to minimize to bubbles' surface area; R is the average pore size of bubble. When the surface tension largely dominates the yield stress of the foam suspension, the capillary number is low, and the bubbles appear as rigid inclusions in the mortar. Therefore, the yield stress of 3DFCs is not affected by the bubbles for gas volume fraction ∅ (Table 3) less than 50. However, when the importance of surface tension decreases, Ca_{τ} increases, and bubbles appear to be soft and easily deformed. A significant reduction of yield stress with ∅ is due to mutual exclusion between the gelling attraction of mortar and the inflated surfactant molecule, with a general increasing trend as a function of foam content.

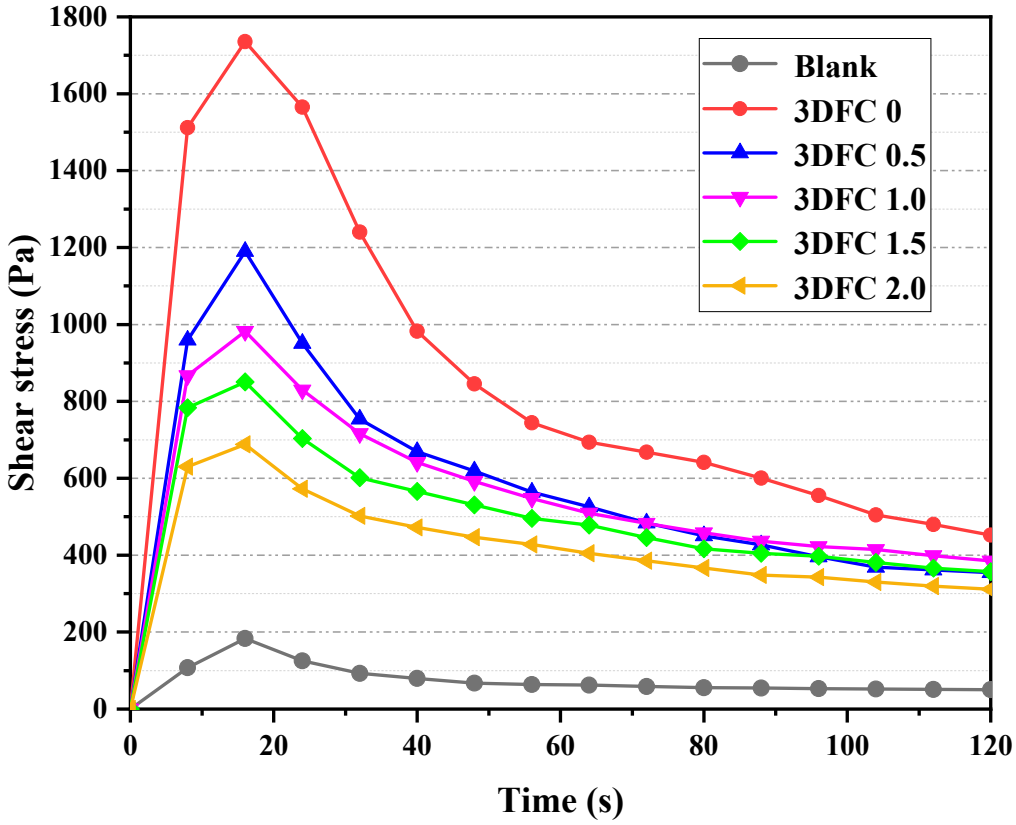

Figure 6. Static yield stress of Blank and 3DFCs.

Table 3. Dimensionless yield stress as a function of the gas volume fraction.

No.	3DFC0	3DFC0.5	3DFC1	3DFC1.5	3DFC2
∅	14.76%	31.49%	32.45%	38.00%	43.07%
$\tau_p(\varnothing)/\tau_p(0)$	0.993	0.965	0.963	0.947	0.93

To go one step further, we list a dimensionless yield stress $\tau_p(\varnothing)/\tau_p(0)$ as a function of ∅ through Equation (2) [34]:

$$\frac{\tau_p(\varnothing)}{\tau_p(0)} = \sqrt{\frac{(1-\varnothing)(5+3\varnothing)}{5-2\varnothing}} \quad (2)$$

Therefore, we calculate the dimensionless yield stress through the above formula in Table 3. It is worthwhile to note all the five values of $\tau_p(\varnothing)/\tau_p(0)$~1, meaning that the yield stress of a bubble suspension is comparable to the one of the suspending emulsion for the range of parameters investigated [34].

3.3. Apparent Viscosity

As an important method to evaluate the rheological properties of 3D printing concrete, viscosity test can directly reflect the buildability of foam mortar. The test results are presented in Figure 7.

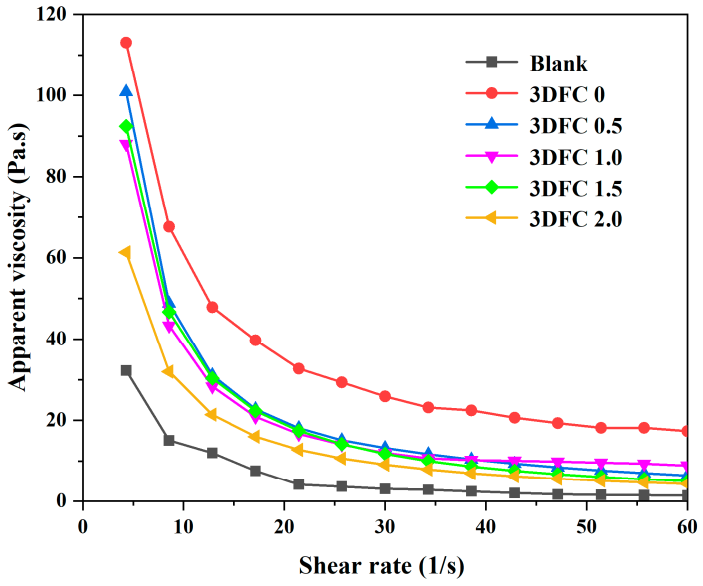

(**a**)

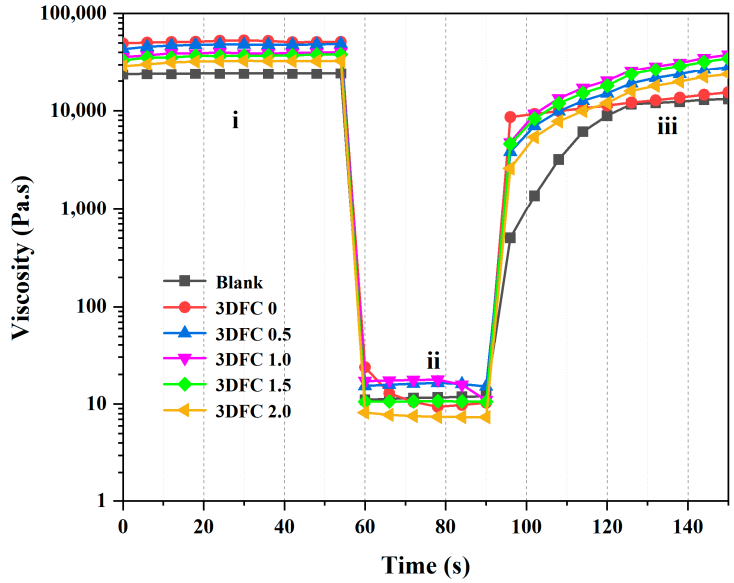

(**b**)

Figure 7. Buildability of Blank and 3DFCs (**a**) Apparent viscosity (**b**) Viscosity recovery.

From Figure 7a, it can be seen that with the increase of shear rate, the apparent viscosity of all mortars decreases gradually. Among them, the blank without HPMC showed the lowest viscosity at each rate stage. With the addition of 0.1% HPMC, the apparent viscosity of 3DFCs increased obviously, especially at the low shear rate stage. The incorporation of HPMC provides a great contribution to the buildability of the foamed mortar. This is consistent with the above-mentioned yield stress test results. Moreover, as shown in Figure 7a, with the increase of surfactant content, the apparent viscosity of 3DFCs decreased gradually at low shear rate but was similar at high shear rate. As demonstrated in previous study, the apparent viscosity of the yield stress fluid is consistent with the yield stress at low-speed shear; that is, the relative decrease of the yield stress will lead to the relative decrease of the apparent viscosity [23].

Figure 7b shows the viscosity recovery curve of blank and 3DFCs. The structural rebuild ability of fresh foam mortar is expressed by comparing the viscosity difference of 3DFCs in stage (i) and stage (iii). From Figure 7b, it can be known that 0.1% HPMC significantly increased the apparent viscosity and viscosity recovery of sample 3DFC0.5 in static state compared with the blank sample. The reason is that the thickening property of cellulose ether induces the flocculation structure of the fresh foam mortar, thereby improving the bubble stability and increasing the structure construction rate. The viscosity recovery of 3DFCs did not change significantly as the addition of surfactant increased from 0.5 to 2%. This shows that the change of pore structure has a weak effect on the viscosity of foam mortar in static state. At the same time, this behavior makes it possible to apply it to industrial applications.

3.4. Buildability

The real buildability of 3DFCs is affected by both yield stress and apparent viscosity, and the schematic diagram of the layer height of 3DFCs in Figure 8 directly shows the buildability of 3D printed pre-foaming concrete. As can be seen from Figure 8, with the increase of the amount of surfactant, the height of the printed products decreases. The sample 3DFC0.5 can print 18 layers continuously at a single time, and the surface of the specimen is smooth and without obvious cracks. The sample 3DFC1.0 and 3DFC1.5 were built with 15 and 14 layers, and 3DFC2.0 was built with 12 layers. The amount of surfactant has a significant effect on buildability of foam mortar, which can explain that when the foam content increases gradually, the porosity and average pore size of the paste increase, and the material structure becomes looser, so that the load it can bear in the fresh state is reduced. Moreover, Figure 9 shows an interval printing process of 3DFC2.0 during a field application. It confirms the possibility of 3D printed pre-foaming concrete in actual production.

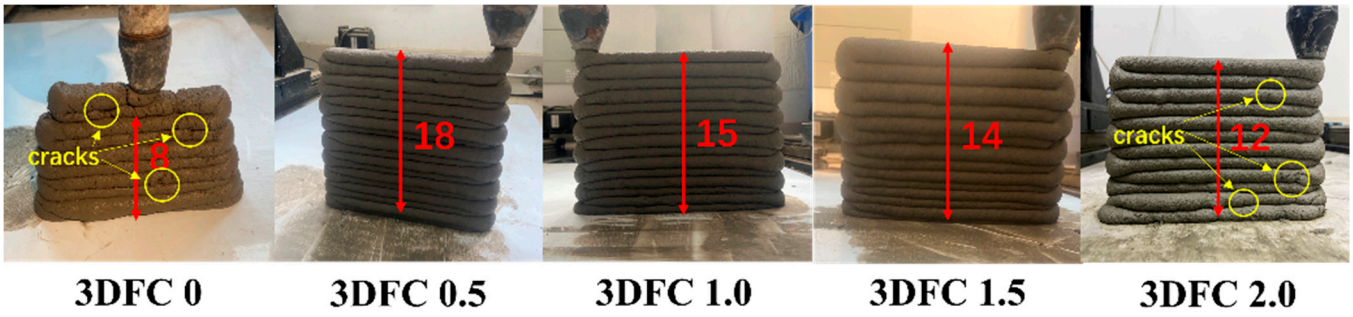

Figure 8. Schematic diagram of the layer height of 3DFCs.

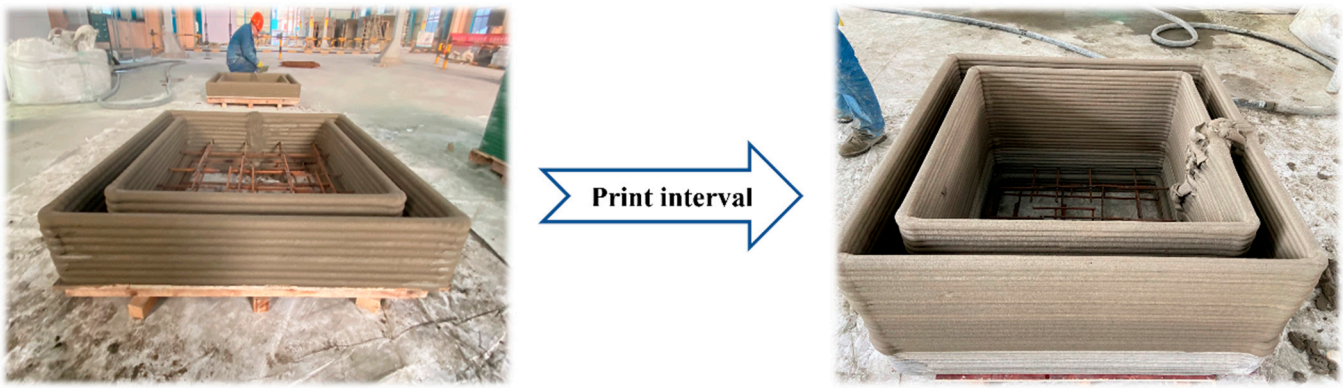

Figure 9. An interval printing process during a field application.

3.5. Pore Structure

The pore structure of 3D printed pre-foaming concrete directly affects the properties of hardened paste, including density, compressive strength and thermal conductivity. Figure 10 presents the pore structure (pore size distribution and volume of Hg intruded) of 3DFCs as measured by Mercury Intrusion Porosimetry (MIP) for 28-day cured foamed mortar. According to the pore size, the pores can be divided into micropores (diameter < 10 nm), mesopores (10–50 nm), capillary pores (50–1000 nm) and macropores (>1000 nm) [35]. Form Figure 10a, it can be seen that compared with 3DFC0, with the increase of surfactant content, there are more capillary pores and macropores in 3DFCs. At a low-level content of surfactant, the sample of 3DFC0.5 added more capillary pores and a small number of macropores. With a higher level of surfactant, the critical pore size of capillary pores of sample 3DFC1, 3DFC1.5 and 3DFC2 is lower than that of 3DFC0. However, the critical pore size for them at macropores increases significantly. This phenomenon can be explained by the rupture between the bubbles introduced by surfactants and the formation of gap separation, resulting in the formation of larger micropores. As can be seen from Figure 10b, the cumulative number of pores of 3DFCs increases with the increase of surfactant dose. This shows that the foam produced by physical foaming of surfactant can obviously increase the number of pores in cement mortar, so as to achieve the purpose of reducing the density of cement mortar.

The scanning electron microscope for 3D printed pre-foaming concrete with two different amounts of surfactants is shown in Figure 11. From the scanning electron microscope images of 50 and 100 magnification, it can be seen that there are a large number of 10–500 μm large pores in the hardened foam mortar, which can not be captured by the MIP test [20]. The micrograph shows the clear difference between the foam pore size and the pore distribution among different hardened mortar. It can be observed from Figure 11, the pore size and the number of large pores are increased with the increase of surfactant dose from 1% to 2%. It is obvious that the increase of foam content increases the pore size and quantity of 3D printed pre-foaming concrete. In addition, it can also be observed that the increase of bubbles leads to the thinning and weakening of the pore wall in the hardened mortar, resulting in the decrease of compressive strength [36].

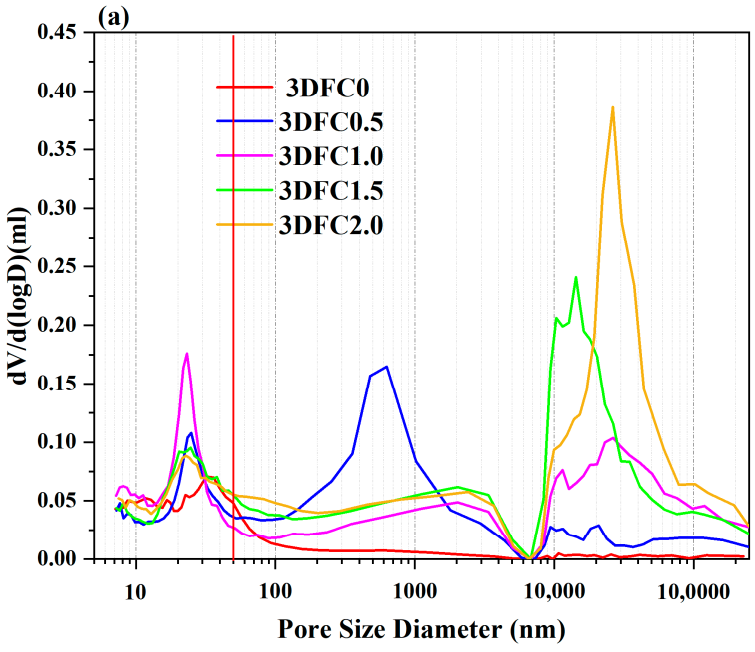

Figure 10. *Cont.*

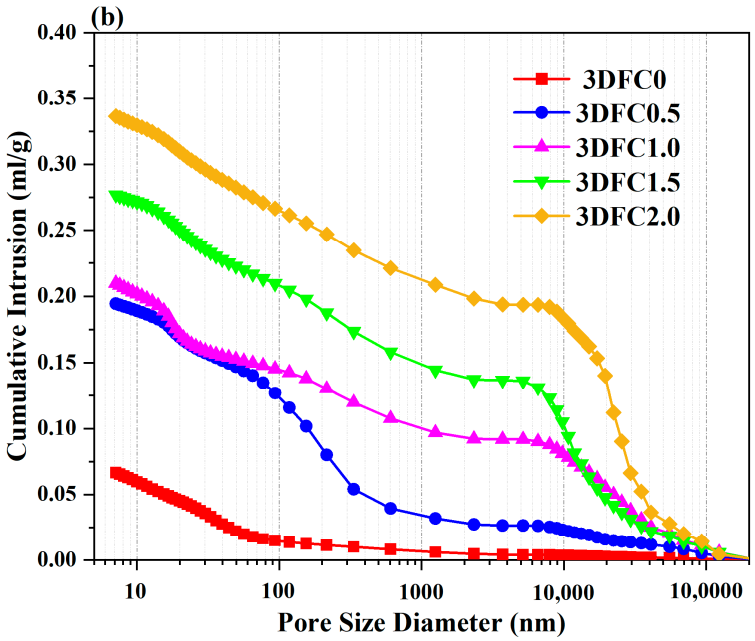

Figure 10. Pore size distribution (**a**) and Volume of Hg Intruded (**b**) of the 3DFCs.

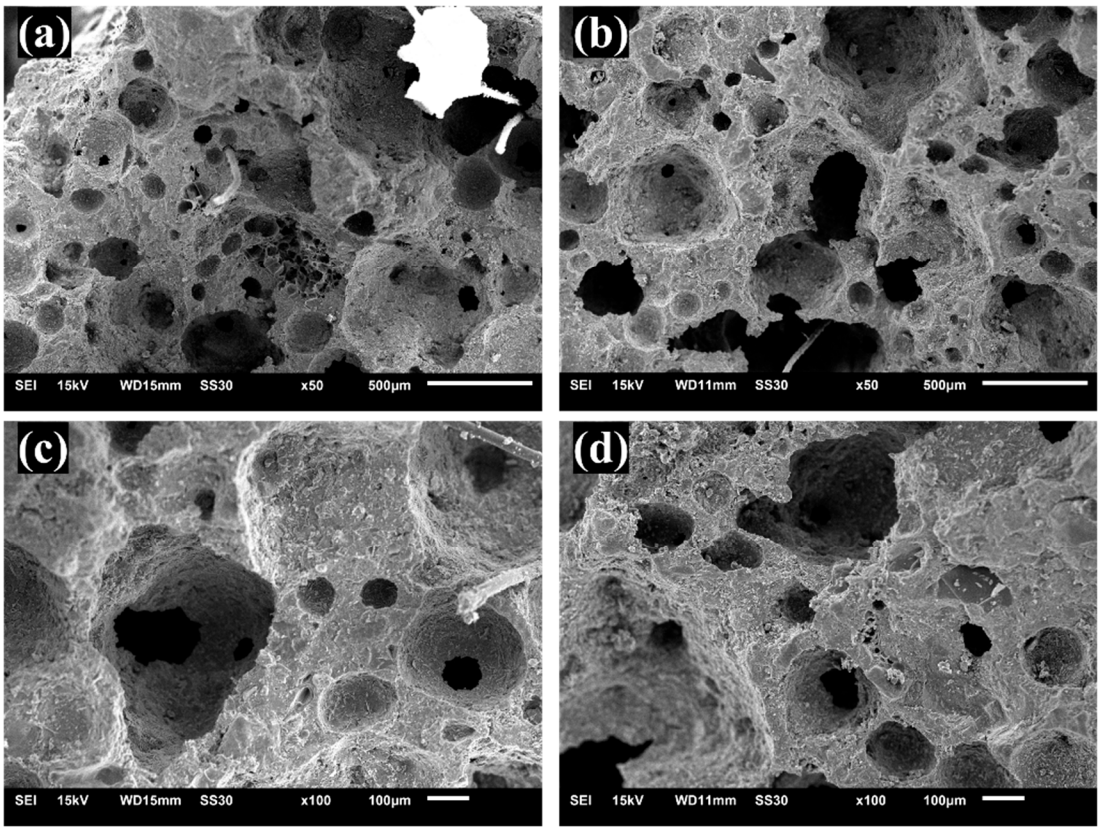

Figure 11. Pore structure of 3DFCs with SEM: (**a**,**c**) surfactant = 1%; (**b**,**d**) surfactant = 2%.

3.6. Compressive Strength, Volume Density

Figure 12 shows the volume density and compressive strength development of all 3DFCs with various dosages of surfactant. Form Figure 12, it can be observed that with the incorporation of surfactant, all the 3DFCs shown significant reduction in volume density,

which is due to the formation of pores in it. For instance, the volume density of sample 3DFC0 without surfactant is 2211 kg/m^3, and it decreases to 1591 kg/m^3 when the addition of surfactant is increased to 0.5 wt.%. The compressive strength of 3DFCs is closely related to its density, both decreasing obviously with the addition of surfactant. The strength performance of printed specimen (i.e., a density of 1591 kg/m^3) improved compared with normal PC foam concrete. This remarkable high strength is mainly attributed to the incorporation of 0.2% fiber, which enhances the compressive strength of 3DFCs by preventing micro-cracks [37,38].

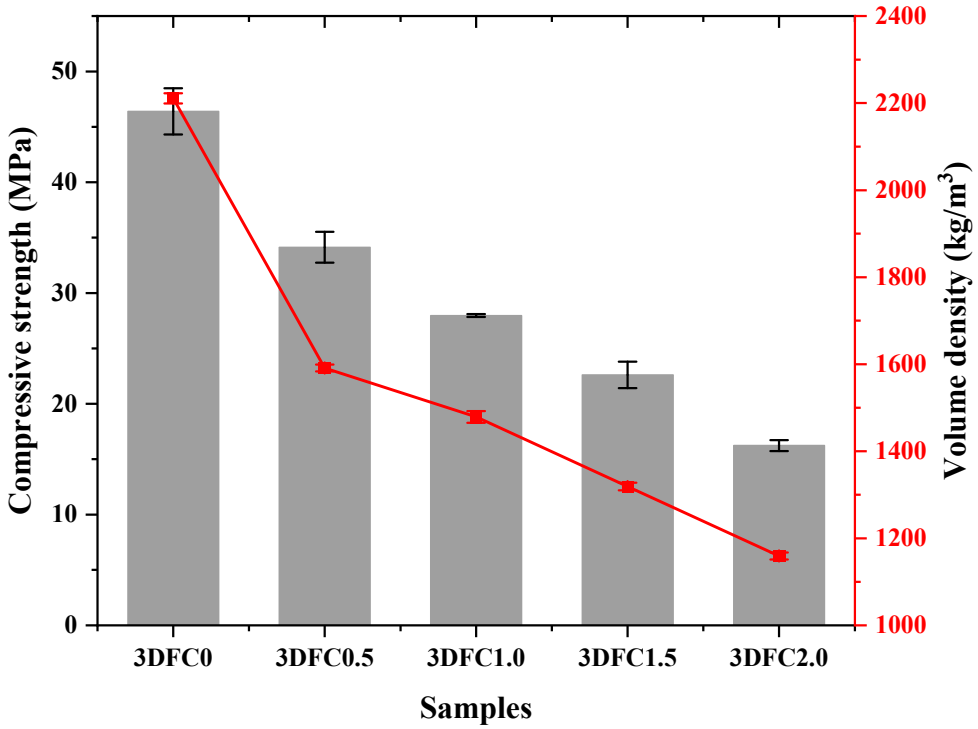

Figure 12. Compressive strength and Volume density of 3DFCs.

3.7. Thermal Conductivity

Thermal conductivity is the main parameter to evaluate the thermal insulation performance of mixtures, which is closely related to the composition, structure and density of mortar [39]. Table 4 shows the thermal conductivity of 3DFCs containing various contents of surfactant at 20 °C. It is easy to find that the thermal conductivity of 3DFCs always decreases with the addition of surfactant, which is probably related to the development of pores in the 3DFCs [40]. It is worth noting that the thermal conductivity of 3DFC containing 0.5 wt.% surfactant is 0.2879 W/(m·K), at a density of 1591 kg/m^3. According to the composition, aggregate and test conditions, the thermal conductivity of 3DFCs in this work is lower than that of existing PC foam concrete registered in the range of 0.6–0.8 W/(m·K), [41]. This is attributed to the decrease of chemically bound water under lower water demand, which provides a more discontinuous gel structure for foamed mortar.

Table 4. Thermal conductivity of 3DFCs of surfactant dosage.

Samples	3DFC0.5	3DFC1.0	3DFC1.5	3DFC2.0
Volume density (kg/m^3)	1600	1480	1320	1160
Thermal conductivity (W/m·K)	0.288	0.287	0.249	0.225

4. Discussion

In foam concrete 3D printing, the rheological properties of fresh foam mortar are crucial for printability and buildability. This is consistent with previous research reports [7,42]. From the results shown in Section 3, when 0.1% HPMC is added to the foam mortar, the yield stress and apparent viscosity of 3DFCs change significantly. This is because the addition of HPMC agglomerates the cement particles together and increases the proportion of large flocculates, thus increasing the yield stress and apparent viscosity of foam mortar [43]. Accordingly, the fluidity and mini-slump of foam mortar also change obviously. Through the actual buildability experiments, it is proved that 0.1% HPMC does make 3DFC have good printability and construction height. This also confirms that fluidity test and mini-slump test can be used as a macroscopic test method to verify the printability of mortar before actual printing [44].

The content of surfactant directly determines the bubble content in fresh foam mortar and the pore structure of hardened mortar, which is very important to the rheological and hardening properties of 3DFCs. At low surfactant concentration, 3DFCs showed higher static yield stress and apparent viscosity (especially in low shear state). Accordingly, it shows higher mini-slump and excellent constructability. With the increase of the dosage of surfactant, the rheological properties of fresh foam mortar change obviously. The static yield stress and apparent viscosity decreased obviously, and macroscopically, it also showed relatively low mini-slump and high fluidity. This change is closely related to the bubble content in foam mortar. In foam mortar, the hydrophilicity and surface charge of cement particles make them adsorb around the bubbles with opposite charge. When the bubble content in 3DFCs is low, the distance between the solid particles is also close. At this time, the particles have a strong van der Waals force and a weak intermolecular repulsion force, which promotes the adsorption between particles and the formation of flocculation structure [7]. With the increase of bubble volume fraction in foam mortar, the connection and penetration of bubbles increase the bubble size, so the interaction force between particles is significantly reduced; thus, the yield stress of foam mortar is reduced [45]. In addition, it can be seen from the buildability experiments that the number of continuous printing layers of 3DFCs decreases obviously with the increase of bubble volume fraction in foam mortar, which may be due to the decrease of yield stress leading to the decrease of load-bearing capacity of 3DFCs [46].

Obviously, as shown in Figure 12, when the amount of surfactant increases from 0 to 2%, the volume density of 3DFCs decreases significantly, accompanied by a sharp decrease in compressive strength. This is related to the development of pore structure in hardened foam mortar [47]. It can be observed from the MIP experiment that the cumulative number of pores in hardened foam mortar increases obviously with the increase of the dosage of surfactant in 3DFCs. It is worth noting that the incorporation of foam significantly increased the number of 10–100 μm macropores in 3DFCs. In addition, the large pores of 100–500 μm in the hardening foam mortar were also observed with SEM experiments. It can be observed that compared with the sample 3DFC1, the pore size and the number of large pores in the sample 3DFC2 are significantly larger. In general, with the increase of surfactant dosage, the total pore number and pore size in hardened foam mortar also increase. The development of pore structure not only causes the volume density change of foam mortar but also contributes to the decrease of thermal conductivity of 3DFCs, which is very beneficial to the practical application of 3D printing lightweight thermal insulation mortar [48,49].

5. Conclusions

This study is aimed to explore the effect of surfactant content on the rheological properties of 3D printed pre-foaming concrete. The changes of mechanical properties, dry density, thermal conductivity and pore structure were measured and discussed. It is expected to provide a valuable reference for the practical application of lightweight pre-foaming concrete in 3D printing. The test and analysis conclusions are as follows:

1. The addition of 0.1 wt.% HPMC to 3DFCs increases the static yield stress and apparent viscosity (especially at low shear rate), thus enhancing the buildability. Although the fluidity of 3DFCs is reduced, its loose and porous internal structure reduces the resistance to pumping, which is suitable for printability.
2. The buildability of 3DFCs containing various dosages of surfactant is evaluated via the static yield stress development, apparent viscosity and viscosity recovery test. Result demonstrates that the incorporation of surfactants reduces the static yield stress and apparent viscosity, but the viscosity recovery rate of all 3DFCs is similar.
3. The MIP test results show that the number of macropores (10–100 μm) and total pores in hardened foam mortar increase obviously with the increase of surfactant. In addition, SEM images show that when the foam content in 3DFCs increases, the pore size and the number of large pores (100–500 μm) in 3DFCs will also increase.
4. The presence of surfactant can effectively reduce the volume density of 3DFCs from 2211 to 1159 kg/m^3 but also weaken the compressive strength of 3DFCs. This is due to the generation of more pores with the addition of surfactant and consequently to the decrease of compressive strength and density. Moreover, the thermal conductivity of 3DFCs decreases slightly from 0.288 to 0.255 W/(m·K), with the gradual increase of surfactant dosage, which is also related to the development of pore structure.

Author Contributions: Y.G.: Scheme design, Data curation, Writing—original draft, Visualization, Investigation. S.H.: Provide inspiration, Funding acquisition, Supervision. H.Y.: Assist in the experiment. All authors have read and agreed to the published version of the manuscript.

Funding: The authors are grateful to the support of this work by the Priority Academic Program Development of Jiangsu Higher Education Institutions (PAPD). We are also grateful for the financial support of Research Funds of Jiangsu Hydraulic Research Institute (2022Z015), Suzhou Science and Technology Program Project (SS202117) and Zhangjiagang Industry-University-Research pre-Research Fund Project (ZKCXY2156).

Conflicts of Interest: The authors declare that they have no known competing financial interests or personal relationships that could have appeared to influence the work reported in this paper.

References

1. Paolini, A.; Kollmannsberger, S.; Rank, E. Additive manufacturing in construction: A review on processes, applications, and digital planning methods. *Addit. Manuf.* **2019**, *30*, 100894. [CrossRef]
2. Bester, F.; van den Heever, M.; Kruger, J.; van Zijl, G. Reinforcing digitally fabricated concrete: A systems approach review. *Addit. Manuf.* **2021**, *37*, 101737. [CrossRef]
3. Panda, B.; Tan, M.J. Experimental study on mix proportion and fresh properties of fly ash based geopolymer for 3D concrete printing. *Ceram. Int.* **2018**, *44*, 10258–10265. [CrossRef]
4. Panda, B.; Unluer, C.; Tan, M.J. Extrusion and rheology characterization of geopolymer nanocomposites used in 3D printing. *Compos. Part B Eng.* **2019**, *176*, 107290. [CrossRef]
5. Panda, B.; Unluer, C.; Tan, M.J. Investigation of the rheology and strength of geopolymer mixtures for extrusion-based 3D printing. *Cem. Concr. Compos.* **2018**, *94*, 307–314. [CrossRef]
6. Jiao, D.; De Schryver, R.; Shi, C.; De Schutter, G. Thixotropic structural build-up of cement-based materials: A state-of-the-art review. *Cem. Concr. Compos.* **2021**, *122*, 104152. [CrossRef]
7. Cho, S.; Kruger, J.; van Rooyen, A.; van Zijl, G. Rheology and application of buoyant foam concrete for digital fabrication. *Compos. Part B Eng.* **2021**, *215*, 108800. [CrossRef]
8. Lv, Q.; Yang, J.; Sun, X.; Tang, H.; Wang, L. Preparation of highly efficient thermal insulating halloysite nanotubes/polyvinyl alcohol composite aerogel based on a simple freeze-drying strategy. *Polym. Compos.* **2022**, *44*, 1648–1657. [CrossRef]
9. Zhang, H.; Yang, J.; Wu, H.; Fu, P.; Liu, Y.; Yang, W. Dynamic thermal performance of ultra-light and thermal-insulative aerogel foamed concrete for building energy efficiency. *Sol. Energy* **2020**, *204*, 569–576. [CrossRef]
10. Zhang, Z.; Provis, J.L.; Reid, A.; Wang, H. Mechanical, thermal insulation, thermal resistance and acoustic absorption properties of geopolymer foam concrete. *Cem. Concr. Compos.* **2015**, *62*, 97–105. [CrossRef]
11. Shah, S.N.; Mo, K.H.; Yap, S.P.; Yang, J.; Ling, T.-C. Lightweight foamed concrete as a promising avenue for incorporating waste materials: A review. *Resour. Conserv. Recycl.* **2021**, *164*, 105103. [CrossRef]
12. Dhasindrakrishna, K.; Pasupathy, K.; Ramakrishnan, S.; Sanjayan, J. Progress, current thinking and challenges in geopolymer foam concrete technology. *Cem. Concr. Compos.* **2021**, *116*, 103886. [CrossRef]

13. Li, T.; Huang, F.; Zhu, J.; Tang, J.; Liu, J. Effect of foaming gas and cement type on the thermal conductivity of foamed concrete. *Constr. Build. Mater.* **2020**, *231*, 117197. [CrossRef]
14. Furet, B.; Poullain, P.; Garnier, S. 3D printing for construction based on a complex wall of polymer-foam and concrete. *Addit. Manuf.* **2019**, *28*, 58–64. [CrossRef]
15. Othuman, M.A.; Wang, Y.C. Elevated-temperature thermal properties of lightweight foamed concrete. *Constr. Build. Mater.* **2011**, *25*, 705–716. [CrossRef]
16. Yang, S.; Wi, S.; Park, J.H.; Cho, H.M.; Kim, S. Novel proposal to overcome insulation limitations due to nonlinear structures using 3D printing: Hybrid heat-storage system. *Energy Build.* **2019**, *197*, 177–187. [CrossRef]
17. Muthukrishnan, S.; Ramakrishnan, S.; Sanjayan, J. Technologies for improving buildability in 3D concrete printing. *Cem. Concr. Compos.* **2021**, *122*, 104144. [CrossRef]
18. Wang, Y.; Jiang, Y.; Pan, T.; Yin, K. The Synergistic Effect of Ester-Ether Copolymerization Thixo-Tropic Superplasticizer and Nano-Clay on the Buildability of 3D Printable Cementitious Materials. *Materials* **2021**, *14*, 4622. [CrossRef]
19. Zhang, C.; Deng, Z.; Chen, C.; Zhang, Y.; Mechtcherine, V.; Sun, Z. Predicting the static yield stress of 3D printable concrete based on flowability of paste and thickness of excess paste layer. *Cem. Concr. Compos.* **2022**, *129*, 104494. [CrossRef]
20. Alghamdi, H.; Neithalath, N. Synthesis and characterization of 3D-printable geopolymeric foams for thermally efficient building envelope materials. *Cem. Concr. Compos.* **2019**, *104*, 103377. [CrossRef]
21. Falliano, D.; De Domenico, D.; Ricciardi, G.; Gugliandolo, E. 3D-printable lightweight foamed concrete and comparison with classical foamed concrete in terms of fresh state properties and mechanical strength. *Constr. Build. Mater.* **2020**, *254*, 119271. [CrossRef]
22. Gu, G.; Xu, F.; Huang, X.; Ruan, S.; Peng, C.; Lin, J. Foamed geopolymer: The relationship between rheological properties of geopolymer paste and pore-formation mechanism. *J. Clean. Prod.* **2020**, *277*, 123238. [CrossRef]
23. Feneuil, B.; Pitois, O.; Roussel, N. Effect of surfactants on the yield stress of cement paste. *Cem. Concr. Res.* **2017**, *100*, 32–39. [CrossRef]
24. Luan, X.; Li, J.; Liu, L.; Yang, Z. Preparation and characteristics of porous magnesium phosphate cement modified by diatomite. *Mater. Chem. Phys.* **2019**, *235*, 121742. [CrossRef]
25. Panda, B.; Sonat, C.; Yang, E.-H.; Tan, M.J.; Unluer, C. Use of magnesium-silicate-hydrate (M-S-H) cement mixes in 3D printing applications. *Cem. Concr. Compos.* **2021**, *117*, 103901. [CrossRef]
26. *ASTM C1437-15*; Standard Test Method for Flow of Hydraulic Cement Mortar. American Society for Testing and Materials: West Conshohocken, PA, USA, 2015.
27. Jiang, J.; Lu, Z.; Niu, Y.; Li, J.; Zhang, Y. Investigation of the properties of high-porosity cement foams based on ternary Portland cement–metakaolin–silica fume blends. *Constr. Build. Mater.* **2016**, *107*, 181–190. [CrossRef]
28. Panda, B.; Tan, M.J. Rheological behavior of high volume fly ash mixtures containing micro silica for digital construction application. *Mater. Lett.* **2019**, *237*, 348–351. [CrossRef]
29. Qian, H.; Hua, S.; Gao, Y.; Qian, L.; Ren, X. Synergistic effect of EVA copolymer and sodium desulfurization ash on the printing performance of high volume blast furnace slag mixtures. *Addit. Manuf.* **2021**, *46*, 102183. [CrossRef]
30. Panda, B.; Ruan, S.; Unluer, C.; Tan, M.J. Improving the 3D printability of high volume fly ash mixtures via the use of nano attapulgite clay. *Compos. Part B Eng.* **2019**, *165*, 75–83. [CrossRef]
31. Lim, J.H.; Panda, B.; Pham, Q.-C. Improving flexural characteristics of 3D printed geopolymer composites with in-process steel cable reinforcement. *Constr. Build. Mater.* **2018**, *178*, 32–41. [CrossRef]
32. *ASTM C349-18*; Standard Test Method for Compressive Strength of Hydraulic-Cement Mortars. American Society for Testing and Materials: West Conshohocken, PA, USA, 2018.
33. Ducloué, L.; Pitois, O.; Tocquer, L.; Goyon, J.; Ovarlez, G. Yielding and flow of foamed metakaolin pastes. *Colloids Surf. A: Physicochem. Eng. Asp.* **2017**, *513*, 87–94. [CrossRef]
34. Ducloué, L.; Pitois, O.; Goyon, J.; Chateau, X.; Ovarlez, G. Rheological behaviour of suspensions of bubbles in yield stress fluids. *J. Non-Newton. Fluid Mech.* **2015**, *215*, 31–39. [CrossRef]
35. Qian, H.; Hua, S.; Yue, H.; Feng, G.; Qian, L.; Jiang, W.; Zhang, L. Utilization of recycled construction powder in 3D concrete printable materials through particle packing optimization. *J. Build. Eng.* **2022**, *61*, 105236. [CrossRef]
36. Pasupathy, K.; Ramakrishnan, S.; Sanjayan, J. Enhancing the properties of foam concrete 3D printing using porous aggregates. *Cem. Concr. Compos.* **2022**, *133*, 104687. [CrossRef]
37. Cheng, C.; Hong, S.; Zhang, Y.; He, J. Effect of expanded polystyrene on the flexural behavior of lightweight glass fiber reinforced cement. *Constr. Build. Mater.* **2020**, *265*, 120328. [CrossRef]
38. Yavuz Bayraktar, O.; Kaplan, G.; Gencel, O.; Benli, A.; Sutcu, M. Physico-mechanical, durability and thermal properties of basalt fiber reinforced foamed concrete containing waste marble powder and slag. *Constr. Build. Mater.* **2021**, *288*, 123128. [CrossRef]
39. Guo, Y.; Liu, Y.; Wang, W.; Zhang, Y.; Wang, Z.; Jiang, L. A study on heat transfer performance of recycled aggregate thermal insulation concrete. *J. Build. Eng.* **2020**, *32*, 101797. [CrossRef]
40. Liu, H.; Zhao, X. Thermal Conductivity Analysis of High Porosity Structures with Open and Closed Pores. *Int. J. Heat Mass Transf.* **2022**, *183*, 122089. [CrossRef]
41. Raj, A.; Sathyan, D.; Mini, K.M. Physical and functional characteristics of foam concrete: A review. *Constr. Build. Mater.* **2019**, *221*, 787–799. [CrossRef]

42. Cho, S.; van Rooyen, A.; Kearsley, E.; van Zijl, G. Foam stability of 3D printable foamed concrete. *J. Build. Eng.* **2022**, *47*, 103884. [CrossRef]
43. Liu, C.; Chen, Y.; Xiong, Y.; Jia, L.; Ma, L.; Wang, X.; Chen, C.; Banthia, N.; Zhang, Y. Influence of HPMC and SF on buildability of 3D printing foam concrete: From water state and flocculation point of view. *Compos. Part B Eng.* **2022**, *242*, 110075. [CrossRef]
44. Dai, S.; Zhu, H.; Zhai, M.; Wu, Q.; Yin, Z.; Qian, H.; Hua, S. Stability of steel slag as fine aggregate and its application in 3D printing materials. *Constr. Build. Mater.* **2021**, *299*, 123938. [CrossRef]
45. Nambiar, E.K.K.; Ramamurthy, K. Air-void characterisation of foam concrete. *Cem. Concr. Res.* **2007**, *37*, 221–230. [CrossRef]
46. Tripathi, A.; Nair, S.A.O.; Neithalath, N. A comprehensive analysis of buildability of 3D-printed concrete and the use of bi-linear stress-strain criterion-based failure curves towards their prediction. *Cem. Concr. Compos.* **2022**, *128*, 104424. [CrossRef]
47. Othman, R.; Jaya, R.P.; Muthusamy, K.; Sulaiman, M.; Duraisamy, Y.; Abdullah, M.; Przybyl, A.; Sochacki, W.; Skrzypczak, T.; Vizureanu, P.; et al. Relation between Density and Compressive Strength of Foamed Concrete. *Materials* **2021**, *14*, 2967. [CrossRef]
48. Li, P.; Wu, H.; Liu, Y.; Yang, J.; Fang, Z.; Lin, B. Preparation and optimization of ultra-light and thermal insulative aerogel foam concrete. *Constr. Build. Mater.* **2019**, *205*, 529–542. [CrossRef]
49. Zhang, D.; Ding, S.; Ma, Y.; Yang, Q. Preparation and Properties of Foam Concrete Incorporating Fly Ash. *Materials* **2022**, *15*, 6287. [CrossRef]